

Supporting Information

For:

A DLVO Model for Catalyst Motion in Metal-assisted Chemical Etching Based upon Controlled
Out-of-Plane Rotational Etching and Force-Displacement Measurements

By

Owen Hildreth

Georgia Institute of Technology
Atlanta, GA 30332

Summary

This document serves to provide supplementary and supporting information necessary or relevant to the understanding of the primary journal article. It will cover such topics as the derivation for the total energy of an elasto-plastic deformation in torsion and bending for prismatic beams, the energy of reactions relevant to Metal-assisted Chemical Etching (MaCE). It will also provide extra data on the 96.4 nm catalysts.

1. Detailed Experimental Procedures	1
1.1 Relevant Literature	1
1.2 EBL Patterned Catalyst	1
1.3 Etching	1
1.4 Observations	1
1.5 Force-Displacement Curves	2
2. Plastic Deformation of Prismatic Beams under Torsion	6
2.1 Relevant Literature	6
2.2 List of Symbols*	6
2.2.1 Subscripts	6
2.2.2 Geometry	6
2.2.3 Material Constants	6
2.2.4 Loading and Moments	6
2.2.5 Elasto-plastic	7
2.3 Geometry Calculations	7
2.4 Geometry	7
2.4.1 Torsion	7
2.4.2 Bending	8
2.5 Torsion of a prismatic beam	8
2.6 Bending	8
3. Energy of Reaction	10
3.1 Relevant Literature	10
3.2 Reaction	10
3.3 Calculate the moles of etched Si	10
3.4 Calculate the maximum amount of available energy	10
4. Tables of Torque, Pressure Gradients and Energy Values for various arm widths	11
4.1 Representative Sample – 147 nm	11
4.2 Percent Elastic Energy	13
5. Graph of Rotation Angle versus arm length for all arm widths	15
6. Electrostatic pressure calculations based upon Hillier paper	16
7. Electrophoretic calculations based upon Paxton papers	18
7.1 List of symbols	18
7.2 Electrophoresis of the first kind	18
7.2.1 Assumptions	18
7.2.2 Equations	19
7.3 Electrophoresis of the second kind	19
7.3.1 Assumptions	20

7.3.2 Equations.....	20
7.4 Force Calculations from Paxton Papers	20
8. Force-Displacement Curves	21

1. Detailed Experimental Procedures

1.1 Relevant Literature

Cappella, B. & Dietler, G. Force-distance curves by atomic force microscopy. *Surface Science Reports* **34**, 1–3, 5–104 (1999).

1.2 EBL Patterned Catalyst

All procedures except for etching, SEM imaging, and AFM measurements were conducted in a class 100 or 10 cleanroom environment; all silicon wafers were handled only in the cleanroom prior to catalyst patterning. All samples were prepared on p-type, 1 – 5 Ω -cm (100) silicon purchased from UltraSil. 350 ± 15 nm, as measured by a Nanospect Reflectometer, of polymethyl methacrylate (PMMA) (MicroChem - PMMA-A6) positive resist was spun onto the silicon wafer and baked for 90 seconds at 180 °C. The PMMA was exposed using a JEOL JBX-9300FS at 100kV accelerating voltage at 2 nA beam current with a base dose of 650 $\mu\text{C}/\text{cm}^2$ and developed for 120 seconds in a 1 : 1 by volume mixture of methyl isobutyl ketone (MIBK) : isopropyl alcohol (IPA) followed by a 120 second rinse in IPA. Approximately 20 nm of PMMA was removed using a descum procedure in a PlasmaTherm RIE SLR using O₂ with Ar carrier gas for 30 seconds at 20W. Sequentially, ~10 nm of Ti followed by ~85 nm of Au was evaporated onto the patterned substrate using a CVC E-beam evaporator. The thickness of the catalyst stack was measured at 92 nm using atomic force microscopy. Metal lift-off consisted of a 24-hour immersion in (Mircoposit - 1165 resist remover) at 80 °C as measured using a mercury thermometer. Substrate was cleaned using AMI (sequential acetone, methanol, IPA rinse), dried using N₂ (Airgas, 99.99%), baked at 180 °C for at least 15 minutes and then allowed to cool to room temperature immediately prior to ~470 nm of maN-2403 (Micro Resist Technologies) negative resist spun onto the substrate which was then baked at 90 °C for 120 seconds followed by exposure using the JEOL JBX-9300FS system under the same conditions as the previous PMMA process. The maN-2403 was developed in MF-319 (2.5 wt.% tetramethyl ammonium hydroxide, TMAH with surfactant – Microposit) for 70 seconds, rinsed for 5 minutes under gently flowing deionized (DI) water, and dried using N₂. Lastly, the samples were descummed in the PlasmaTherm RIE SLR immediately prior to MaCE for 60 seconds under the same conditions as earlier.

1.3 Etching

Samples were removed from the cleanroom and immersed in a dilute solution of 1:100 by vol. HF:H₂O (Aldrich – 48 wt.% : deionized, 15.5M Ω) to ensure a uniform, hydrophobic surface prior to MaCE. MaCE was conducted in the dark using a stagnant $\rho = 90^{13.8}$ etchant solution of HF:H₂O₂:H₂O = 4:1.3:2.8 ml (Aldrich – 48wt% : Aldrich – 35 wt.% : DI water). The etchant was carefully applied to the sample to ensure that the etchant solution flowed slowly over the silicon wafer during application; in our previous work we found that the etchant solution can move the catalyst during the etching process if it is applied carelessly. The etchant solution was kept stagnant during etching and the only opportunities for external excitation were when the etchant was applied or removed from the sample. No bubbles were observed on the Si or catalyst region during etching of maN-2403 pinned catalysts while bubbles were observed during etching of non-pinned catalyst structures in our earlier work. Once etching was complete the sample was immersed for 5 minutes in ample DI water maintained at room temperature (~27 °C) to halt the etching process.

1.4 Observations

All samples were imaged using the in-lens detector of a Zeiss LEO 1550 Thermally Assisted Field Emission (TFE) Scanning Electron Microscope (SEM) operating at 10kV accelerating

voltage and 3 – 4 mm working distance. The thickness of the catalyst stack was measured using a Bruker Dimension Edge SPM in tapping mode.

1.5 Force-Displacement Curves

Two different fluids were tested. 1) dilute HCl solution with a measured pH of 0.62 to match the pH of a $\rho = 90^{13.8}$ etchant solution 2) dilute HCl solution with HF added to 1 wt%, and DI water. All solutions were made using DI water with a measured resistivity of 15.5 M Ω .

Two substrates were tested, a silicon substrate and a thermal SiO₂ on silicon substrate. The silicon substrates were the same as those used for the out-of-plane rotational structures. To measure the force-displacement curves between SiO₂ and the AFM tips a 107 nm thick thermal oxide measured using a Nanospec Reflectometer was grown on the same silicon wafers as above using dry O₂ at 1100 °C for four hours. As the wafer was prepared well before use, the substrate was cleaned for 10 minutes in a 200 W O₂ plasma and then 10 × 30 mm² samples were scribed from the 100 mm wafer for use.

NPG-10 tips coated top and bottom with Cr/Au were used in the Force-displacement curves. The tip radius was measured at 30 nm using the LEO 1550 at 5:00 AM to minimize noise from any vibrations within the building (i.e. cooling fans). The sensitivity in $\mu\text{m}/\text{volt}$ of each tip was measured by gathering a force-displacement curve between the cantilever and a fresh silicon substrate in air. The measured sensitivities were between 0.095 and 0.1078 $\mu\text{m}/\text{V}$ across the tips used with a 0.002 $\mu\text{m}/\text{V}$ range across multiple measurements for individual tips. Next the spring constant of the AFM tips was measured using the thermal tune method in air for spring constants between 0.056 and 0.902 N/m.

Force-displacement curves were taken for each substrate first in air, then in DI water, and then in the target fluid. The force-displacement curves within water were found to be consistent within each tip/substrate set. 1 – 3 μm long force-displacement curve was taken at an approach velocity that was around 0.15 – 0.25 $\mu\text{m}/\text{sec}$ were taken for each of the substrate/fluid sets.

The pressure-displacement curves were calculated based a 2 nm contact radius calculated using a Hertzian model with a 30 nm tip radius, as measured in Figure 1, and a 1 μN trigger force. The calculated contact radius, a , is given by:

$$a = \sqrt[3]{\frac{RF}{K}}$$
$$\frac{1}{K} = \frac{3}{4} \left(\frac{1-\nu_s^2}{E_s} + \frac{1-\nu_i^2}{E_i} \right)$$

where: R is the radius of the tip, F is the force between the tip and the surface which was conservatively set at the trigger force of 1 μN as this will overestimate the contact radius and underestimate the pressure. The adjusted modulus, K , is calculated from the Piosson's ratio, ν , and Young's Modulus, E , of the sample and indenter (denoted by the subscripts s and i).

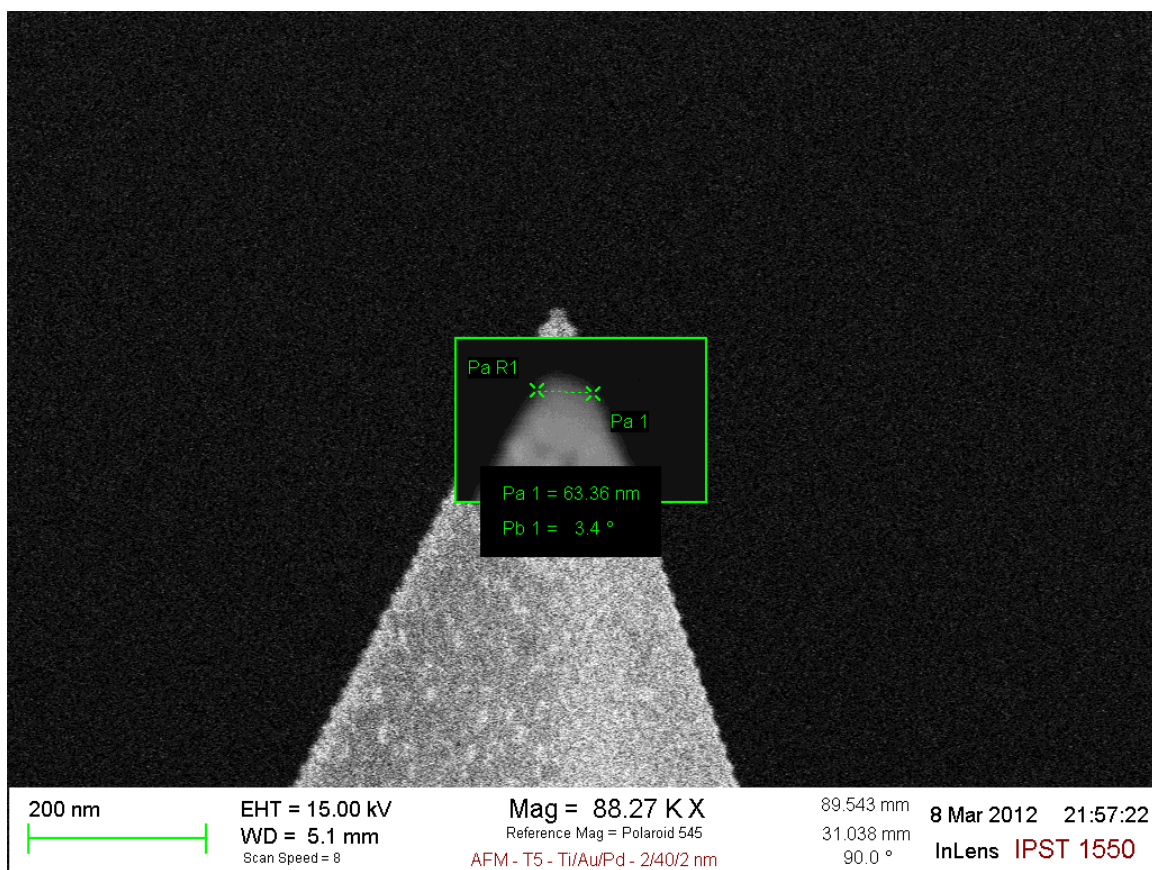


Figure 1. SEM micrograph of AFM tip used in Force-Displacement curves.

2. Etch rate and current density of Ag, Au, and Pt catalysts

The graphs in Figure 2 plot the calculated current density based upon mass loss measurements for Pt and Ag catalysts for P(100) - 0.086 Ω -cm and 1.59 Ω -cm silicon. Notice that the current density for the Pt catalyst is over ten times larger than the Ag catalysts. Also, the lower 0.0086 Ω -cm silicon shows a higher current density, indicating that silicon resistivity does play a role determining etch rate, although the current density does not scale linearly with resistivity. More importantly, these results show that the etching rate is kinetically limited for highly concentrated etchants (not shown here are results with Pd catalysts, which etch at 20 – 50 times faster than Pt catalysts). As such, only a thin layer of Pt catalyst is necessary to achieve extremely high etch rates. This fact was exploited in our work to design a Ti/Au/Pt catalyst structure that had the high etch rate needed to induce out-of-plane rotation without using Pt as the core material. This avoids damage to the electron resist caused by the boiling temperature of Pt. The data from these current density calculations is also used to examine if electrophoresis could be the driving force for catalyst motion as detailed in our manuscript. Table 1 summarized the etch depth and rate for Ag, Au, and Pt catalysts for a variety of dopant levels and crystallographic orientations.

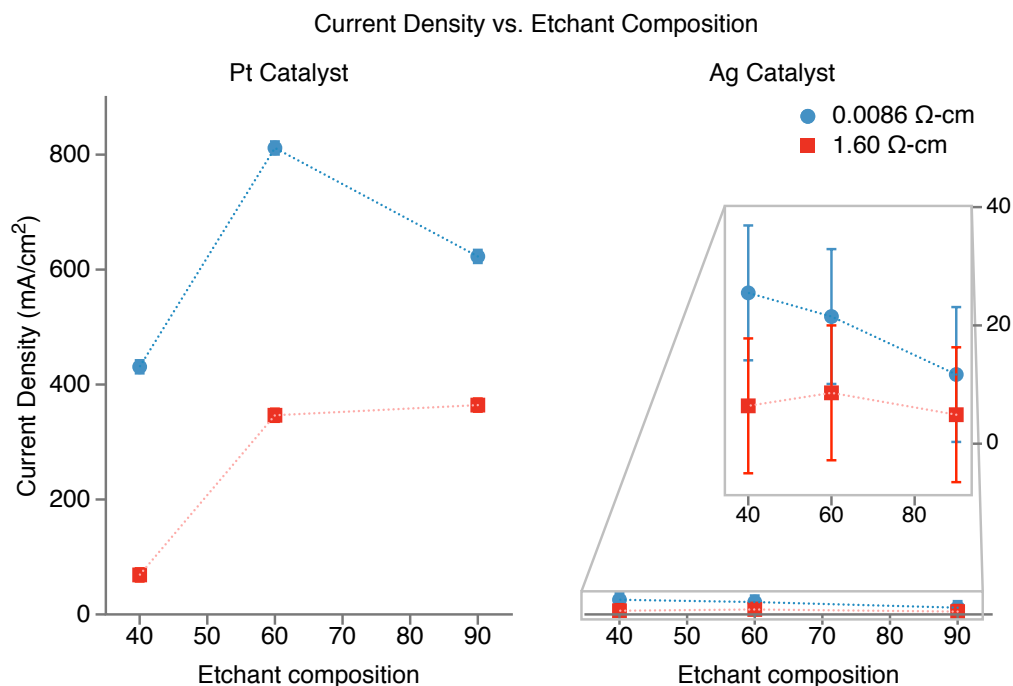


Figure 2. Graphs of the current density of Pt and Ag catalysts etched for 2 minutes in $\rho = 40^{5.0}$, $60^{7.9}$, and $90^{13.8}$ etchants. Note that the dashed lines serve solely to aid the eye and that the error bars for the Pt catalysts are too small to see at this scale.

Table 1. Etch depth and rate for Ag, Au, and Pt catalysts for various silicon dopant levels and orientations. Samples were etched for 10 seconds in a HNO_3/HF = 9013.8 etchant. It is clear that the rate varies dramatically with catalyst selection, with Ag etching on the order of 10 – 30 nm/sec, Au from 20 – 70 nm/sec, and Pt around 10 times higher at 500 – 1,000 nm/sec. It is important to note that the error associated with these measurements may be large because the etching time was only 10 seconds and it is unknown how long it takes to “quench” the etching process.

Substrate Type (orientation) - Ω -cm	Etch Depth [μm]			Etch Rate [nm/sec]		
	Ag	Au	Pt	Ag	Au	Pt
P(100) - 0086	0.10	0.70	5.5	10	70	550
P(100) - 1.60	0.30	0.45	10	30	45	1,000
P(111) - 1.53	-	0.23	4.7	-	23	470

3. Plastic Deformation of Prismatic Beams under Torsion

3.1 Relevant Literature

Kaluszky, S. "Plasticity: Theory and Engineering Applications." First ed. Studies in Applied Mechanics. New York, NY: Elsevier, 1989. 147 - 158, 264 - 275. (Chapters 4 and 6)

3.2 List of Symbols*

*note – some of these symbols have been changed from those used in the reference to maintain consistency between the Supporting Information and the Published Article along with increasing clarity. For example, w is used as the width instead of a , as in the referenced document.

3.2.1 Subscripts

- e elastic regime
- p plastic regime
- a catalyst arm geometry
- c center catalyst geometry (i.e. horseshoe or asymmetric rectangle, subscript)

3.2.2 Geometry

- w = beam/arm width (m)
- t = beam/arm thickness (m)
- l_a = beam/arm length (m)
- l_c = center catalyst length (m)
- I = Area Moment of Inertia (m⁴)
- J = Polar Moment of Inertia (m⁴)

- y_{max} = maximum lateral deflection (m)
- θ = angle of deflection (radians)
- θ_r = resting angle of deflection (radians)
- θ_m = max. measured angle of deflection (radians)

3.2.3 Material Constants

- E = Modulus of elasticity (Pa)
- G = Shear modulus of elasticity (Pa)
- σ_o = Yield stress (Pa)
- τ_o = Yield shear stress (Pa)

3.2.4 Loading and Moments

- p = pressure load on beam (Pa)
- q = $p \cdot w$ = distributed load on beam (N/m)
- L = total load on beam (N)
- T = torsion/moment on beam (N-m)

3.2.5 Elasto-plastic

M_e	= elastic limit moment	(Pa)
M_p	= plastic limit moment	(Pa)
T_e	= elastic limit torque	(N-m)
T_p	= plastic limit torque	(N-m)
q_e	= plastic limit distributed load	(Pa)
p_e	= plastic limit pressure	(Pa)

3.3 Geometry Calculations

Area Moment of Inertia

$$I = \frac{wh^3}{12} \quad (1)$$

Polar Moment of Inertia

$$J = \frac{wh}{12}(w^2 + h^2) \quad (2)$$

3.4 Geometry

3.4.1 Torsion

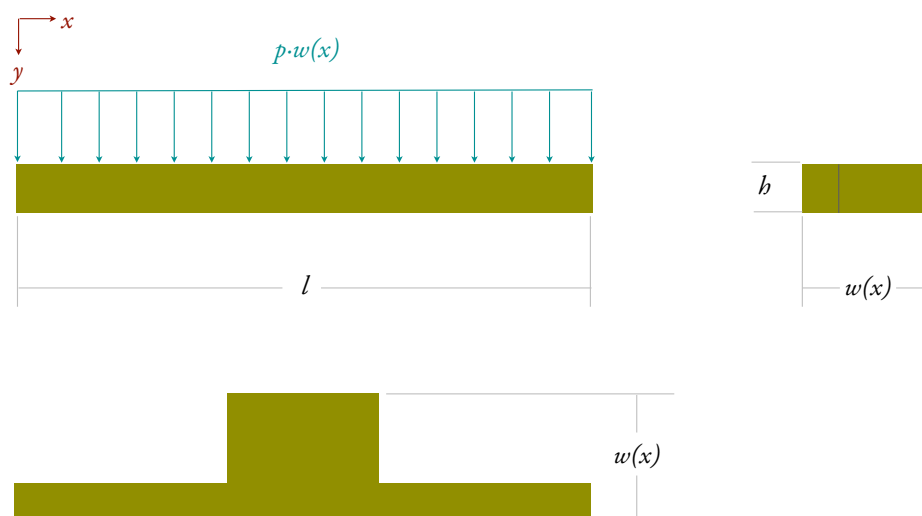


Figure 3. Schematic of catalyst geometry for torsion.

3.4.2 Bending

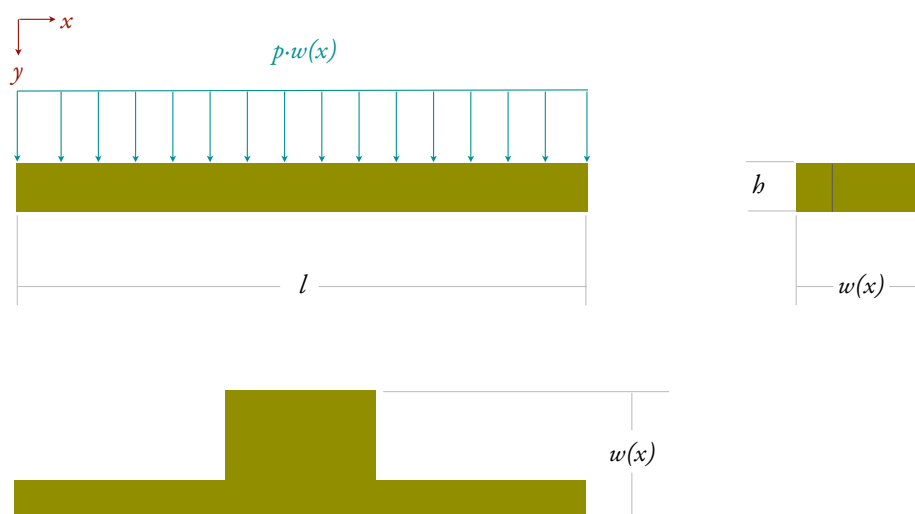


Figure 4. Schematic of catalyst geometry for bending

3.5 Torsion of a prismatic beam

Assumptions:

- 1) Center catalyst is a rigid body and does not bend or twist
 - a. This assumption is validated by the SEM images that show that the center catalyst structure does not noticeably twist
- 2) Pressure is applied across the catalyst thickness in the regions where the catalyst is in contact with the silicon
 - a. This assumption is valid in an Derjaguin and Landau, Verwey and Overbeek (DVLO) model, surface energy model and electrophoretic model
- 3) Torque generated due to the pressure gradient across the catalyst structure is transmitted directly to the arms of the catalyst
- 4) Torque is applied symmetrically about the catalyst

$$T_p = \frac{4}{3} T_e \quad (3)$$

$$T_p = \frac{wh^2}{6} \left(3 - \frac{h}{w}\right) \tau_o \quad h \leq w \quad (4)$$

$$T_p = \frac{1}{2} p_p w_{cat}^2 \quad (5)$$

3.6 Bending

Assumptions:

- 1) Catalyst deforms plastically
 - a. Calculations put the plastic displacement limit at 60 nm, our catalyst displaced ~800 nm
- 2) Catalyst is simply supported
 - a. Over 90% of catalysts showed deflection that is characteristic of a simply supported structure

The elastic and plastic limit moments are defined as:

$$M_e = \frac{wt^2}{6} \sigma_o \quad (6)$$

$$M_p = \frac{wh^2}{4} \sigma_o \quad (7)$$

for a simply supported beam with a distributed load, $q = p \cdot w(x)$, gives an elastic limit linear load of:

$$q_e = p_e \cdot w = \frac{8M_e}{l^2} = \frac{4wh^2}{3l^2} \sigma_o \quad (8)$$

$$p_e = \frac{4h^2}{3l^2} \sigma_o \quad (9)$$

$$p_p \cdot w = \frac{8M_p}{l^2} = \frac{2wh^2}{l^2} \sigma_o \quad (10)$$

$$p_p = \frac{2h^2}{l^2} \sigma_o \quad (11)$$

Notice that the elastic limit pressure does not depend on the width of the catalyst. This gives an elastic limit displacement, $y_e(x)$ of:

$$y_e(x) = \frac{5}{384} \frac{p_e w l^4}{EI} = \frac{1}{4} \frac{l^2}{Eh} \sigma_o \quad (12)$$

the elastic limit pressure, plastic pressure limit, and elastic limit displacement for the catalyst with dimensions: $h = 130$ nm, $l = 4160$ nm, $E = 50$ GPa are: $p_e = 0.13$ MPa, $p_p = 0.20$ MPa, $y_e = 107$ nm. The typical catalyst displacement for the simply supported structures was ~ 800 nm, showing that the structures were deforming in a pure plastic state.

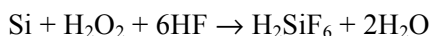
4. Energy of Reaction

This section will outline how the calculations for the amount of available chemical energy do to the H₂O₂ reduction and Si oxidation. The calculations were conducted for a sample that rotated through a full 180°, forming a half-cylinder that was 1040 nm long and 1040 nm in diameter.

4.1 Relevant Literature

4.2 Reaction

The overall reaction in Metal-assisted Chemical Etching (MaCE)



The enthalpy of reaction is defined as:

$$\Delta H_{\text{rxn}}^{\circ} = \sum \Delta_f H_{\text{products}}^{\circ} - \sum \Delta_f H_{\text{reactants}}^{\circ} \quad (13)$$

Table 2. Enthalpy of Formations

Chemical	$\Delta_f H^{\circ}$ (kJ/mol)
HF	-269
H ₂ O	-286
H ₂ O ₂	+329
H ₂ SiF ₆	-586
Si	0

This provides an enthalpy of reaction of: -19.8 kJ/mol.

4.3 Calculate the moles of etched Si

Volume of the silicon removed is the same as a half-cylinder

$$V = \frac{1}{2} \pi r^2 l \quad (14)$$

for the geometry used:

$$r = 0.5 \times D = 0.5 \times 1040 \text{ nm} = 520 \text{ nm} = 520 \text{E-9 m}$$

$$l = 1040 \text{ nm} = 1040 \text{E-9 m}$$

$$V = 1.4 \text{E-19 m}^3 = 1.4 \text{E-13 cm}^3$$

$$N_{\text{mol}}^{\text{Si}} = \rho_{\text{Si}} V_{\text{removed}}^{\text{Si}} \text{AMU}_{\text{Si}} \quad (15)$$

Table 3. Values used to calculate amount of etched Si

Symbol	Value	Units
ρ_{Si}	2.329	(g/cm ³)
V_{removed}	1.4×10^{-13}	(cm ³)
AMU_{Si}	28	(g/mol)

The number of moles of Si removed in the process was:

$$N_{\text{mol}}^{\text{Si}} = 3.4 \times 10^{-14} \text{ mol}$$

4.4 Calculate the maximum amount of available energy

The maximum amount of available energy, U_{rxn}

$$U_{\text{rxn}} = \Delta H_{\text{rxn}}^{\circ} \cdot N_{\text{mol}}^{\text{Si}} \quad (16)$$

$$U_{\text{rxn}} = -6.7 \times 10^{-10} \text{ J}$$

5. Tables of Torque, Pressure Gradients and Energy Values for various arm widths

5.1 *Representative Sample – 147 nm*

The following tables provide the material and geometric values used to calculate the Plastic Limit Torque, pressure gradient, elastic, plastic and total energies for 150 nm wide catalysts over 40 test arm lengths based upon the measured maximum rotation angle.

Table 4. Material and Geometric values that are constant across all samples

Variable	Symbol	Units	Value
Shear Modulus	G	Pa	27000000000
Max Shear	τ_o	Pa	100000000
Length	L	nm	1040
Thickness	b	nm	103
Arm Width	w	mm	147
Plastic Limit Torque	T_p	N-m	5.93×10^{-14}
Pressure Gradient	p	MPa	1.7

Table 5. Measured rotation angle as a function of arm length along with the calculated elastic limit, elastic, plastic and total energies.

Row	Arm Length	Resting Rotation Angle	Maximum Measured Angle	Elastic Limit (degrees)	Energy Min Plastic N-m	Plastic ? Y/N	Energy Elastic J	Energy Plastic H	Total Energy H	%Elastic %
1	0	0	0	0.00	-	1	-	0	-	-
2	45	0	0	0.07	1.82E-17	0	0.0	0.0	0.0	-
3	90	0	0	0.14	3.63E-17	0	0.0	0.0	0.0	-
4	135	0	0	0.21	5.45E-17	0	0.0	0.0	0.0	-
5	179	0	0	0.28	7.22E-17	0	0.0	0.0	0.0	-
6	224	0	0	0.35	9.04E-17	0	0.0	0.0	0.0	-
7	269	0	0	0.42	1.09E-16	0	0.0	0.0	0.0	-
8	314	0	0	0.49	1.27E-16	0	0.0	0.0	0.0	-
9	359	0	0	0.56	1.45E-16	0	0.0	0.0	0.0	-
10	404	0	0	0.63	1.63E-16	0	0.0	0.0	0.0	-
11	449	0	0	0.70	1.81E-16	0	0.0	0.0	0.0	-
12	494	0	0	0.77	1.99E-16	0	0.0	0.0	0.0	-
13	538	0	0	0.84	2.17E-16	0	0.0	0.0	0.0	-
14	583	0	0	0.91	2.35E-16	0	0.0	0.0	0.0	-
15	628	0	0	0.98	2.53E-16	0	0.0	0.0	0.0	-
16	673	0	0	1.05	2.71E-16	0	0.0	0.0	0.0	-
17	718	0	0	1.12	2.90E-16	0	0.0	0.0	0.0	-
18	763	0	0	1.19	3.08E-16	0	0.0	0.0	0.0	-
19	808	0	0	1.26	3.26E-16	0	0.0	0.0	0.0	-
20	853	0	0	1.33	3.44E-16	0	0.0	0.0	0.0	-
21	897	21.1	22.1	1.40	3.62E-16	1	3.62E-16	2.15E-14	2.18E-14	1.7
22	942	0.0	0.0	1.47	3.80E-16	0	0.0	0.0	0.0	-
23	987	0.0	0.0	1.54	3.98E-16	0	0.0	0.0	0.0	-
24	1032	6.3	6.3	1.61	4.16E-16	1	4.16E-16	4.88E-15	5.29E-15	7.9
25	1077	0.0	0.0	1.68	4.34E-16	0	0.0	0.0	0.0	-
26	1122	49.5	49.5	1.75	4.53E-16	1	4.53E-16	4.94E-14	4.99E-14	0.91
27	1167	53.5	53.5	1.82	4.71E-16	1	4.71E-16	5.35E-14	5.39E-14	0.87
28	1212	53.5	54.0	1.89	4.89E-16	1	4.89E-16	5.39E-14	5.44E-14	0.90
29	1256	36.4	36.4	1.96	5.07E-16	1	5.07E-16	3.57E-14	3.62E-14	1.40
30	1301	51.5	51.5	2.03	5.25E-16	1	5.25E-16	5.12E-14	5.17E-14	1.01
31	1346	33.7	33.7	2.10	5.43E-16	1	5.43E-16	3.27E-14	3.33E-14	1.63
32	1391	117.8	117.8	2.17	5.61E-16	1	5.61E-16	1.20E-13	1.20E-13	0.47
33	1436	51.0	51.0	2.24	5.79E-16	1	5.79E-16	5.05E-14	5.11E-14	1.13
34	1481	71.5	180.0	2.31	5.97E-16	1	5.97E-16	1.84E-13	1.84E-13	0.32
35	1526	124.1	124.1	2.38	6.16E-16	1	6.16E-16	1.26E-13	1.27E-13	0.49
36	1571	0.0	0.0	2.45	6.34E-16	0	0.0	0.0	0.0	-
37	1615	121.4	180.0	2.52	6.51E-16	1	6.51E-16	1.84E-13	1.84E-13	0.35
38	1660	90.0	180.0	2.59	6.70E-16	1	6.70E-16	1.84E-13	1.84E-13	0.36
39	1705	82.6	180.0	2.66	6.88E-16	1	6.88E-16	1.83E-13	1.84E-13	0.37
40	1750	90.0	180.0	2.73	7.06E-16	1	7.06E-16	1.83E-13	1.84E-13	0.38

5.2 Percent Elastic Energy

To justify an plastic deformation model the percent elastic energy was calculated and plotted in a histogram for 91 samples as shown in Figure 5. The elastic energy was found to account for less than 2% of the total energy for 70% of the samples.

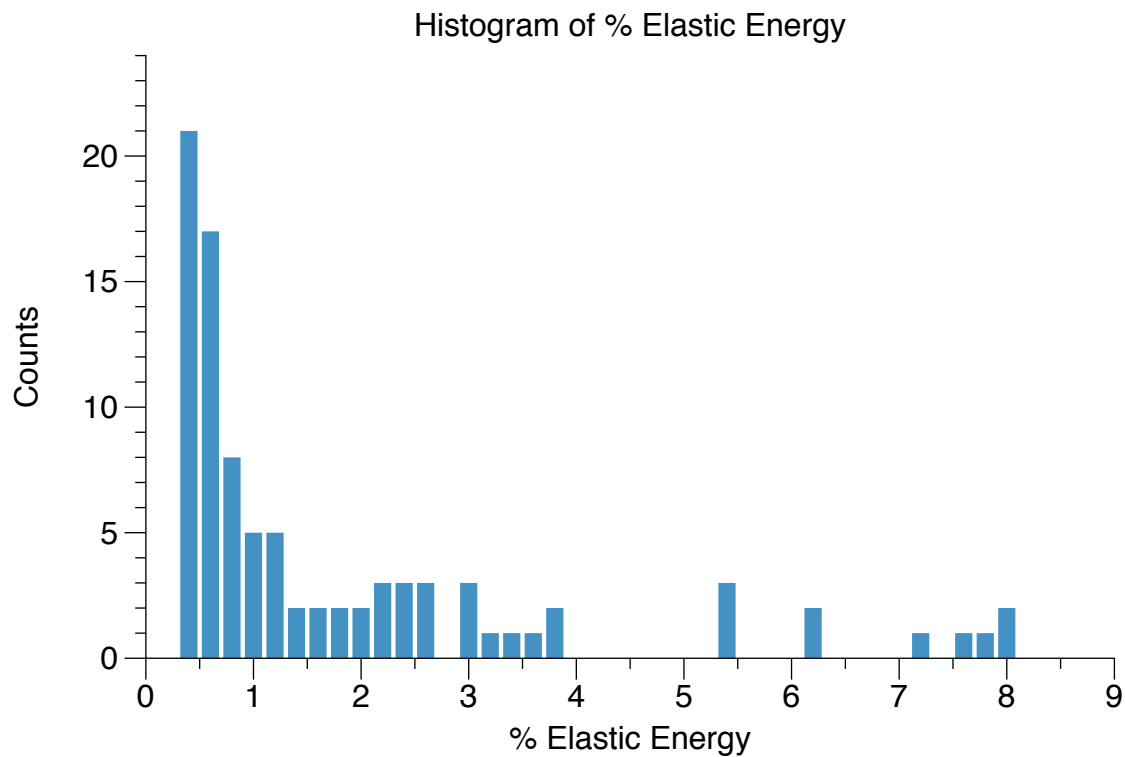


Figure 5. Histogram showing the % elastic energy from the elasto-plastic model for 91 samples. Notice that the elastic energy accounts for less than 2% of the total energy for 70% of the samples.

6. Graph of Rotation Angle versus arm length for all arm widths

graph of 6 arm widths shows that the rotation angle varies linearly with arm length and inversely with arm width. Two arm widths, 147 and 160 were removed for the publication solely to improve the clarity of the published figure.

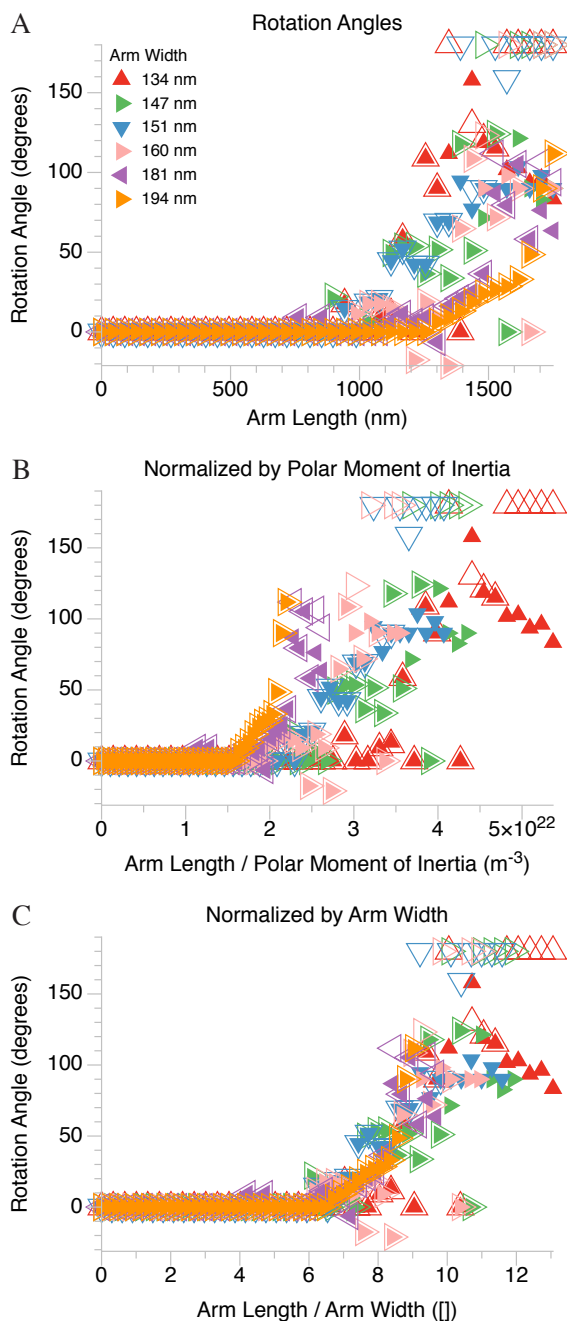


Figure 6. Graphs of the measured resting (\blacktriangle) and maximum (\triangle) rotation angles versus A) arm length; B) normalized by the polar moment of inertia; C) normalized by the arm width.

7. Electrostatic pressure calculations based upon Hillier paper

- 1) A.C. Hillier, S. Kim, and A.J. Bard. "Measurement of double-layer forces at the electrode/electrolyte interface using the atomic force microscope: potential and anion dependent interactions." **J. Phys. Chem.** vol. 100 pp. 18808-18817, 1996

Hillier examined the electrostatic and Van der Waals forces between a silica sphere and a gold surface under acidic 5.5 pH solutions with applied potentials ranging from -700 – 100 mV. The spheres range in size from 10 – 20 μm . The largest normalized attractive and repulsive forces measured were -0.4 and 1.5 mN/m respectively as shown in Figure 8. Hillier also showed calculated forces using the DLVO model (Dergaguin – Landau – Verwy – Overbeek) which had much higher values than those measured, this difference was attributed to "an overestimation of the Hamaker constant, an ill-defined location for the plane of surface charge and the presence of short-range repulsive solvent forces." Since theoretical calculations using DLVO theory overestimated the attractive forces for both Hillier's and quickly increased into the 10 terapascal range in our own preliminary calculations, we chose to use Hillier's data as a rough estimate on the magnitude of the Van der Waals and electrostatic forces may be in our system. There are clearly a number of key differences between Hillier's system and ours, such as silica spheres interacting with a Au surface versus Au particles interacting with a silicon surface, pH of the solution and composition of the solution. However, Hillier does show that, while the interaction distance does change dramatically with electrolyte composition, the ultimate force measured depends mostly on the applied potential.

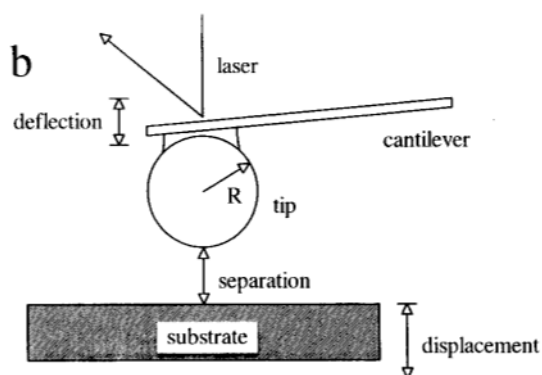


Figure 7. Schematic from Hillier, Figure 1b. Shows basic experimental setup. R_{tip} ranges from 10 – 20 μm . We assume 10 μm to calculate the pressure distribution on the tip to conservatively overestimate the pressure gradient on the AFM sample tip.

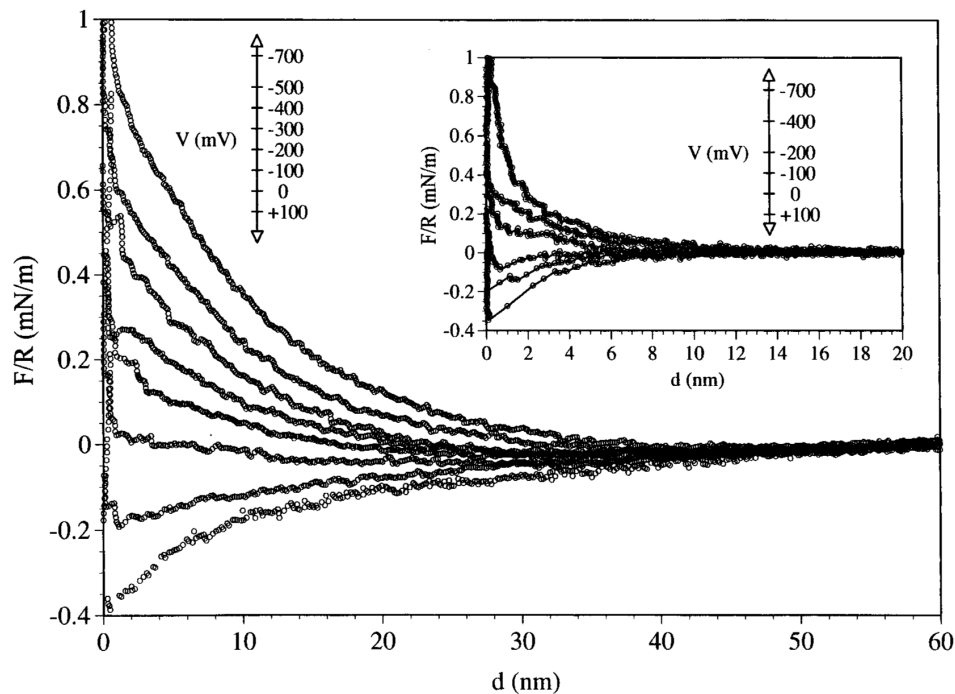


Figure 8. Force between silica sphere and gold electrode in an aqueous solution of 10.3 M KCl at 25 °C and $\text{pH} \approx 5.5$ as a function of the applied potential at gold electrode. The curves correspond to, from top to bottom, electrode potentials of -700 , -500 , -400 , -300 , -200 , -100 , 0 , and 100 mV (vs SCE). Electrostatic repulsion decreases as the electrode potential increases from -700 to 100 mV. Inset: force data for silica sphere and gold substrate in 10.2 M KCl solution.

We assume a conservatively low estimate on the tip radius of $10 \mu\text{m}$ and 10 nm as the distance that the electrostatic and Van der Waals forces are active then the calculated pressure gradient is conservatively high and ranges from $6,400$ to $24,000$ Pa.

R = radius of AFM tip
 h = interaction distance
 F_{measured} = normalized force on AFM tip as measured by Hillier
 F_{cap} = absolute force on AFM tip
 S_{cap} = surface area of spherical cap = area of interaction between AFM tip and surface
 P_{cap} = pressure gradient on AFM tip

R = $10 \mu\text{m}$ = $10 \times 10^{-6} \text{ m}$
 h = 10 nm = $10 \times 10^{-9} \text{ m}$
 F_{measured} = 1.5 mN/m = $1.5 \times 10^{-3} \text{ N/m}$
 F_{cap} = 15 nN = $15 \times 10^{-9} \text{ N}$

S_{cap} = $2\pi Rh$ = $6.28 \times 10^{-13} \text{ m}^2$
 P_{cap} = $F_{\text{cap}}/S_{\text{cap}}$ = $24,000 \text{ Pa}$

8. Electrophoretic calculations based upon Paxton papers

- 1) W.F. Paxton, K.C. Kistler, C.C. Olmeda, A. Sen, S.K. St Angelo, Y.Y. Cao, T.E. Mallouk, P.E. Lammert, and V.H. Crespi. "Catalytic nanomotors: Autonomous movement of striped nanorods." *J. Am. Chem. Soc.* vol. 126 (41), pp. 13424-31, **2004**
- 2) W.F. Paxton, P. Baker, T. Kline, and Y. Wang. "Catalytically induced electrokinetics for motors and micropumps." *J. Am. Chem. Soc.* vol. 128 (46), pp. 14882 - 14888, **2006**

References relevant to electrophoresis:

- 1) *Interfacial Electrodynamics and Electrophoresis*. 1st ed. Published by Marcel Dekker, New York, **2002**, pp. 124 – 250

All symbols and equations were taken from the above book and is an excellent reference on electrophoresis of the first and second kind.

8.1 List of symbols

a = radius of particle
 k = conductivity of the bulk solution

E = electric field
 F = force on particle
 J = current density
 P = pressure gradient on particle
 U = bulk velocity of particle

ϵ_r = relative permittivity
 ϵ_0 = permittivity of vacuum
 κ = Debye length
 η = viscosity of electrolyte
 μ = electrophoretic mobility
 ζ = zeta potential

Ψ_0 = surface potential

8.2 Electrophoresis of the first kind

Classical electrokinetic phenomena are caused by the electrical double layer existing at electrified interfaces. Both the velocity of the liquid along the charged, immobile interface (electro-osmosis) and the velocity of a particle mobile in a liquid (electrophoresis) are functions of surface potential and strength of the external electric field. At low voltage the electrokinetic phenomena is a linear function of the strength of the electric field. Ions within the double layer migrate in the electric field, propelling the particle in the opposite direction.

8.2.1 Assumptions

- 1) particles are non-conducting
- 2) particles are charged
 - a. charge can be induced by electric field
- 3) zeta potential, ζ , is small

a. on order of tens to hundreds of mV

8.2.2 Equations

$F_e = \sigma E$	Force/area on charged particle from electric field
$\kappa = \left(\frac{I}{\epsilon_r \epsilon_o kT} \sum_{i=1}^N z_i e^2 n_i^\infty \right)^{\frac{1}{2}}$	Debye Length of double layer
$E_o \approx \frac{\Psi_o}{\kappa^{-1}} = \Psi_o \cdot \kappa$	Approximate electric field at particle surface
$E_o = \frac{\sigma}{\epsilon_r \epsilon_o}$	Electric field at particle surface
$\Psi_o = \frac{\sigma}{\epsilon_r \epsilon_o \cdot \kappa}$	Electric Potential at particle surface
$F_h = \eta \frac{U}{\kappa^{-1}}$	Viscous force on particle surface per unit area
$\dot{v} = \frac{U}{\kappa^{-1}} = \dot{v} = \frac{dv}{dx}$	Velocity gradient
$U = \mu \cdot E_{ }$	Velocity as a function of electrophoretic mobility and electric field
$\mu = \frac{\epsilon_r \epsilon_o}{\eta} \zeta \cdot f(\kappa a)$	General form of electrophoretic mobility
$2/3 \leq f(\kappa a) \leq 1$	correction factor range

There are two key differences between MaCE and a classical electrokinetic phenomena. Firstly, in MaCe, the particles are electrically conducting. The second difference is that the potential across the particle surface can be on the order of thousands of mV. Paxton's electrophoretic model used a modified version of a classical electrophoretic system but with the external electric field replaced by an induced electric field caused by the mobility/conductivity difference between the H^+ ions flowing on the outside of the particle as compared to the mobility/conductivity of the electrons, e^- , flowing inside the particle. This sets up an electric field that where $E = J/k$ where J = current density due to electrochemical reaction and k = conductivity of the build solution.

$$U_{ep} = \frac{\mu J}{k}$$

8.3 Electrophoresis of the second kind

Electrophoresis of the second kind is also known as fast electrophoresis. Particle motion in standard electrophoresis is caused by fluid flow within the double layer surrounding a charged particle in an external electric field. For electrophoresis of the second kind a secondary double layer is created behind the quasi-equilibrium primary double layer due to strong electric fields. This secondary double layer contains an induced space charge that increases the ion migration velocity. For fast electrophoresis, the velocity of the particle is a function of the square of the electric field, leading to very high velocities.

8.3.1 Assumptions

- 1) current flows through particle
- 2) unipolar conduction through the particle (i.e. only ions, electrons (e^-) or holes (h^+))
- 3) higher conductivity through particle (K_p) than through surrounding medium (K_m)
- 4) high electric field gradients
- 5) current density in the over-limit regime
 - a. required to form and induced space charge region near the surface behind the quasi-equilibrium double electric layer
- 6) $2Ea \gg \Phi_{critical}$
 - a. $\Phi_{critical} \sim 100$ mV for ion conductors
 - b. $\Phi_{critical} \sim 1.5$ V for electron (e^-) or hole (h^+) conductors

8.3.2 Equations

$$2Ea \gg \Phi_{critical}$$

requirement for fast electrophoresis

$$\zeta_{effective} \sim \Phi \sim 2Ea$$

effective ζ for fast electro-osmotic flow over flat membrane

$$\mu = \frac{\epsilon_r \epsilon_o}{\eta} \zeta_{eff} \cdot f(\kappa a)$$

electrophoretic mobility for fast-electrophoresis

$$= \frac{\epsilon_r \epsilon_o}{\eta} (2Ea) \cdot f(\kappa a)$$

$$U = \mu \cdot E_{||}$$

$$= \frac{\epsilon_r \epsilon_o}{\eta} f(\kappa a) \cdot (aE^2)$$

velocity for fast-electrophoresis

8.4 Force Calculations from Paxton Papers

Paxton calculated the force on the Pt/Au striped nanorods as 72.0 mN/m for the 2 μ m long nanorods travelling at 17 μ m/sec in “*Catalytic nanomotors: Autonomous movement of striped nanorods.*” This translates to an absolute force and pressure gradient of 144 nN and 38,000 Pa respectively. The electric field for this system can be resolved from Paxton’s later paper *Catalytically induced electrokinetics for motors and micropumps* and is 10.6 V/cm for the 17 μ m/sec particle velocities. If we apply a fast-electrophoresis model where particle velocity and force is proportional to the square of the electric field, then the resulting pressure gradient is 0.4 MPa, which is very similar to the pressure gradients measured in our system. However, this calculation does not take the 10^5 magnitude increase in ionic conductivity for the MaCE system as compared to Paxton’s system. This reduces the electrophoretic pressure gradient down to less than 1 kPa.

9. Force-Displacement Curves

The raw displacement-displacement and force-displacement curves are shown in Figure 9. These curves show the DVLO encompassed forces operating over 4 nm. The pressure-displacement curves were

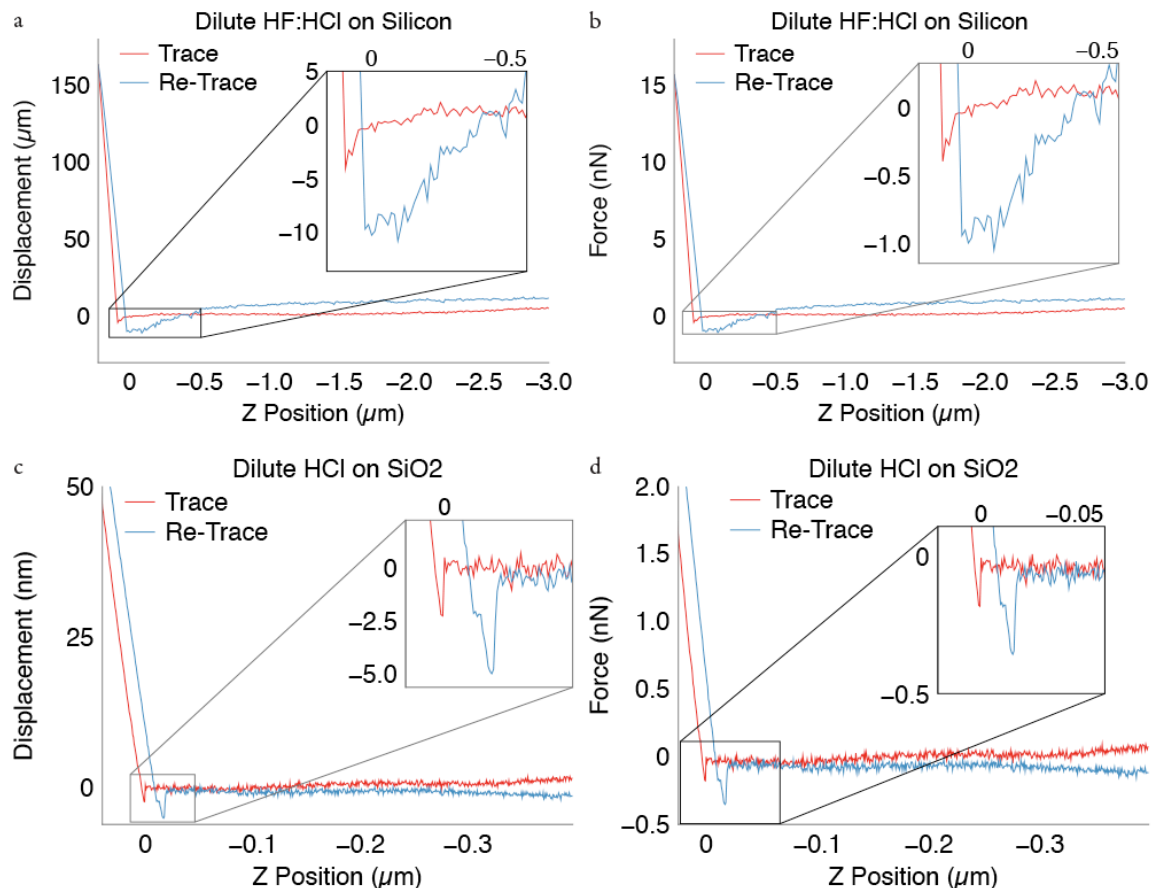


Figure 9. Raw Displacement-Displacement and Force-Displacement curves showing measured displacement and calculated force in nN. (a-b) between Au tip and silicon substrate in dilute HF:HCl showing pull-on forces of 300 pN operating over 3.2 nm; (c-d) between an Au tip and a SiO₂ in dilute HCl showing pull-on forces of 220 pN operating over 2.0 nm.